Icarus 251 (2015) 332–338

Contents lists available at ScienceDirect

Icarus

journal homepage: www.elsevier.com/locate/icarus

Enumeration of Mars years and seasons since the beginning of telescopic exploration

Sylvain Piqueux [a,*], Shane Byrne [b], Hugh H. Kieffer [c,d], Timothy N. Titus [e], Candice J. Hansen [f]

[a] Jet Propulsion Laboratory, California Institute of Technology, M/S 183-601, 4800 Oak Grove Drive, Pasadena, CA 91109, USA
[b] University of Arizona, Lunar and Planetary Laboratory, Tucson, AZ 85721-0092, USA
[c] Celestial Reasonings, 180 Snowshoe Ln., POB 1057, Genoa, NV 89411-1057, USA
[d] Space Science Institute, 4750 Walnut Street, Suite 205, Boulder, CO 80301, USA
[e] Astrogeology Science Center, United States Geological Survey, 2255 N. Gemini Dr., Flagstaff, AZ 86001, USA
[f] Planetary Science Institute, 1700 E. Fort Lowell, Suite 106, Tucson, AZ 85719, USA

ARTICLE INFO

Article history:
Received 6 August 2014
Revised 10 November 2014
Accepted 9 December 2014
Available online 10 January 2015

Keywords:
Mars
Mars, polar caps
Mars, atmosphere
Mars, climate

ABSTRACT

A clarification for the enumeration of Mars years prior to 1955 is presented, along with a table providing the Julian Dates associated with $L_s = 0°$ for Mars years −183 (beginning of the telescopic study of Mars) to 100. A practical algorithm for computing L_s as a function of the Julian Date is provided. No new science results are presented.

Well before the start of the martian robotic exploration in the 1960s with the US Mariner (Leighton et al., 1965) and soviet Mapc (Mars) programs (Florenski et al., 1975), Earth-based telescopic observations led several generations of scientists to the understanding that both the surface and the atmosphere of Mars are dynamic units changing over the scale of hours to seasons. Bright clouds and hazes were observed to appear and disappear at specific locations and local times (Slipher, 1927; Wright and Kuiper, 1935; Martin and Baum, 1969); local, regional, and global dust storms were monitored and recognized to be prevalent at specific seasons and areas (Antoniadi, 1930; de Vaucouleurs, 1954; Golitsyn, 1973); variations of the surface albedo and color far from the poles were observed locally and regionally (Antoniadi, 1930; Slipher, 1962); the seasonality of both polar caps was tracked for indications of inter-annual and global scale environmental changes (James et al., 1992). A fuller description of historic telescopic observations is given by Martin et al. (1992).

The characterization of these large-scale phenomena was limited by the low spatial resolution of available data, observational biases due to orbital constraints on Earth-based observations, and limitations in telescopic remote sensing techniques. The advent of robotic exploration has revolutionized our view of Mars as a dynamic system: globally available high spatial and temporal resolution datasets relying on various remote sensing and in situ techniques have opened the door to systematic surveys, and to the characterization of inter-seasonal and inter-annual variability (see a few examples in Smith, 2004; Geissler, 2005; Titus, 2005; Benson et al., 2006). Studies of modern dynamic processes have also become possible e.g., Sullivan et al. (2001), Russell (2008), Byrne et al. (2009), Verba et al. (2010), Hansen (2011), McEwen et al. (2011) and Daubar et al. (2013). Concomitantly, the enormous amount of data available has fueled a large body of dynamical numerical models emulating geological processes occurring at the scale of seconds (e.g., Rafkin et al., 2001; Michaels, 2006; Mangold et al., 2010) to centuries e.g., Byrne and Ingersoll (2003) and Thomas et al. (2009).

While a consensus has unanimously emerged in the community to define martian local hours as 1/24th fraction of a Mars day ("sol"), and seasons as the aerocentric longitude of the Sun, the Mars community has only recently adopted an absolute enumeration of individual martian years (referred to as MY in this paper, not to be confused with Mega years). Under this system designed by Clancy et al. (2000) for their inter-annual data comparison needs, MY 1 started on April 11 1955 (Temps Universel Coordonné, UTC at 00:00:00) at $L_s = 0°$ (the year of the great 1956 dust storm, L_s being measured from the intersection of the plane of Mars equator and the plane of its orbit, corresponding to

* Corresponding author. Fax: +1 818 354 2494.
E-mail address: Sylvain.Piqueux@jpl.nasa.gov (S. Piqueux).

http://dx.doi.org/10.1016/j.icarus.2014.12.014
0019-1035/

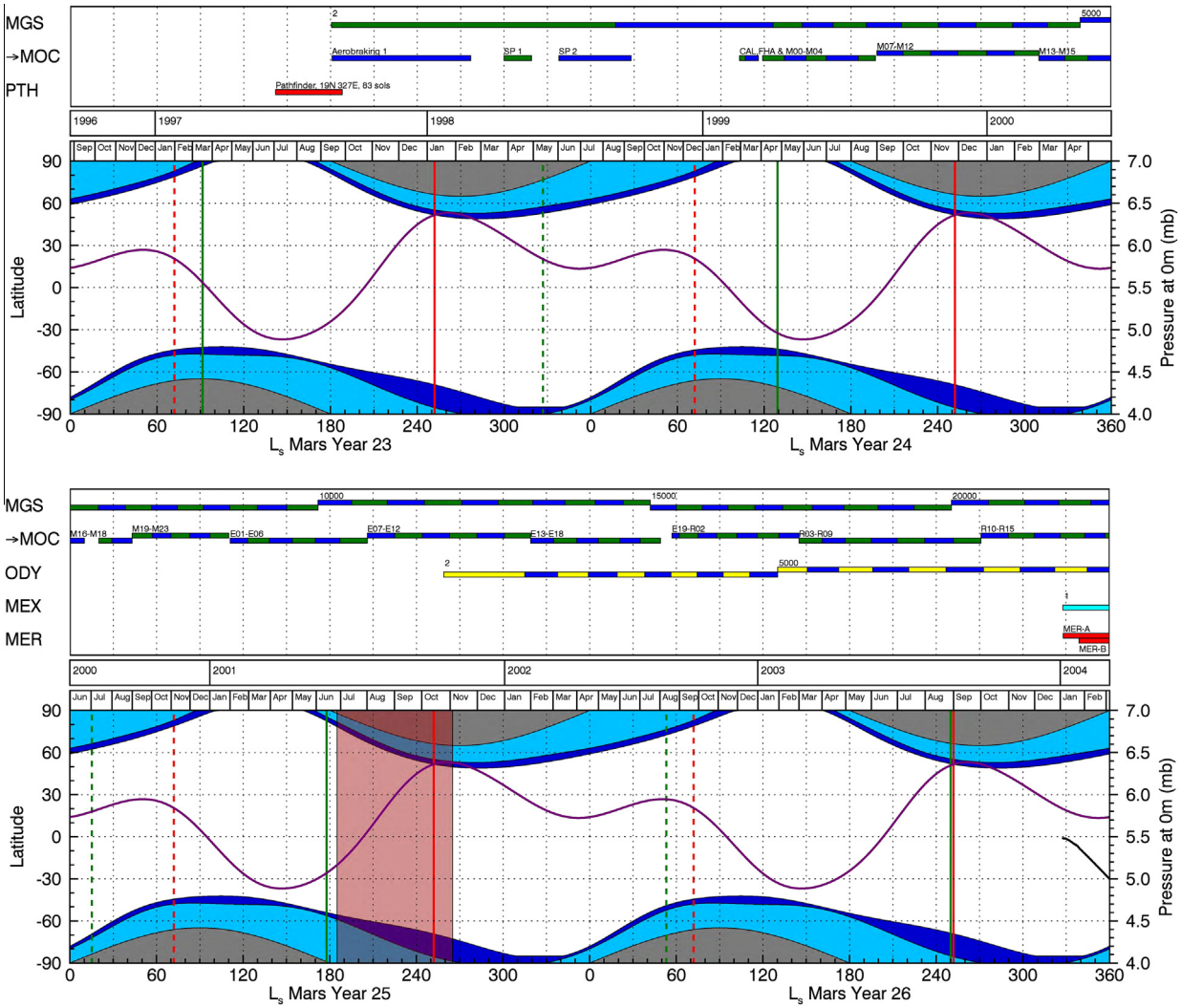

Fig. 1. Martian graphical calendar from MY 23 to MY 32, with periods of activity of robotic missions (top) and global scale phenomena (bottom). ODY: Mars Odyssey; MER: Mars Exploration Rovers (MER A: Spirit and MER B: Opportunity); MRO: Mars Reconnaissance Orbiter; MSL: Mars Science Laboratory/Curiosity; MEX: Mars Express; MGS: Mars Global Surveyor; PTH: Mars Pathfinder; PHX: Phoenix Lander. Additional information can be found in Soderblom and Bell (2008). The different data acquisition phases of the Mars Orbiter Camera (MOC) onboard MGS are indicated, as their nomenclature is not directly related to MGS orbit numbers. Black line indicates MEX periapsis latitude. Orbit numbers are indicated for orbiters (based on data archived in NASA's Navigation and Ancillary Information Facility – NAIF – website, at ftp://naif.jpl.nasa.gov/pub/naif/MEX/kernels/orbnum/ORMM_MERGED_01098.ORB for MEX, ftp://naif.jpl.nasa.gov/pub/naif/MRO/kernels/spk (information contained in *.norb files) for MRO, ftp://naif.jpl.nasa.gov/pub/naif/M01/kernels/spk (information contained in *.norb files) for ODY, ftp://naif.jpl.nasa.gov/pub/naif/pds/data/mgs-m-spice-6-v1.0/mgsp_1000/extras/orbnum and ftp://naif.jpl.nasa.gov/pub/naif/pds/data/mgs-m-spice-6-v1.0/mgsp_1000/extras/orbnum/mgs (information contained in *.nrb files) for MGS pre-mapping and mapping orbits. MOC dates can be extracted from https://starbase.jpl.nasa.gov/archive/mgs-m-moc-na_wa-2-dsdp-l0-v1.0/mgsc_0010/index/cumindx.tab and http://pds-imaging.jpl.nasa.gov/data/mgs-m-moc-na_wa-2-sdp-l0-v1.0/mgsc_1578/index/cumindex.tab. For MOC, additional information is available at http://www.msss.com/moc_gallery/moc_subphases.html. Duration of surface activities for rovers and landers are indicated in sols. Gray shading shows the extent of the polar night. Blue shading indicates the extent of the seasonal polar caps (light blue is the minimum extent, and dark blue is the maximum extent) (Titus, 2005). Atmospheric pressures at 0 m elevation is indicated in purple, from Tillman et al. (1993). Global dust storms are indicated in salmon. Dates of aphelion and perihelion are fixed at L_s 252 and 72 and indicated in red (dashed and solid lines, respectively) and dates of conjunction and opposition relative to the Earth are in green (dashed and solid lines respectively) and calculated using the NAIF Spacecraft Planet Instrument C-Matrix Events (SPICE) toolkit (http://naif.jpl.nasa.gov/naif/toolkit.html). All time conversions between terrestrial and martian time done using the algorithms of Allison and McEwen (2000).

the vernal equinox, see Allison and McEwen (2000), their Fig. 1) and lasted until Mars completed a full revolution around the Sun, i.e. February 26 1957 UTC (beginning of MY 2). The Mars community quickly adopted this enumeration system at a time when climatological records were starting to be established and because it greatly clarifies and simplifies the comparison with Julian calendar dates. However, an ambiguity has remained regarding the count of MY prior to 1955. Such dates in the recent martian past are regularly used in the literature, primarily for cyclical processes spanning a few martian decades (see for example references in Titus et al., 2008).

Here we extend Clancy et al.'s (2000) definition by defining MY 0 (May 24 1953), and any previous MY with "–" as a prefix (i.e., MY −1 starts on July 7th 1951, −2 on August 19 1949, etc.). For numerical calculations, the inclusion of MY 0 is a significant simplification. In addition, most time keeping systems start at 0. Mars calendar alternatives with different origins have been informally proposed (e.g., Wood and Paige, 1992; Tamppari et al., 2000; Smith et al., 2001), without being widely accepted and were as arbitrary as the one adopted here.

Table 1 provides a correspondence between the beginning of every MY ($L_s = 0°$) since the first known telescopic observations of Mars by Galileo (circa 1610 , MY −183) to MY 100, the civil calendar, and days from the origin of the modern astronomical time system, J2000.0 (Julian Date (JD) 2451545.0). A similar table, but without the MY assignments, is presented in Kieffer et al. (1992);

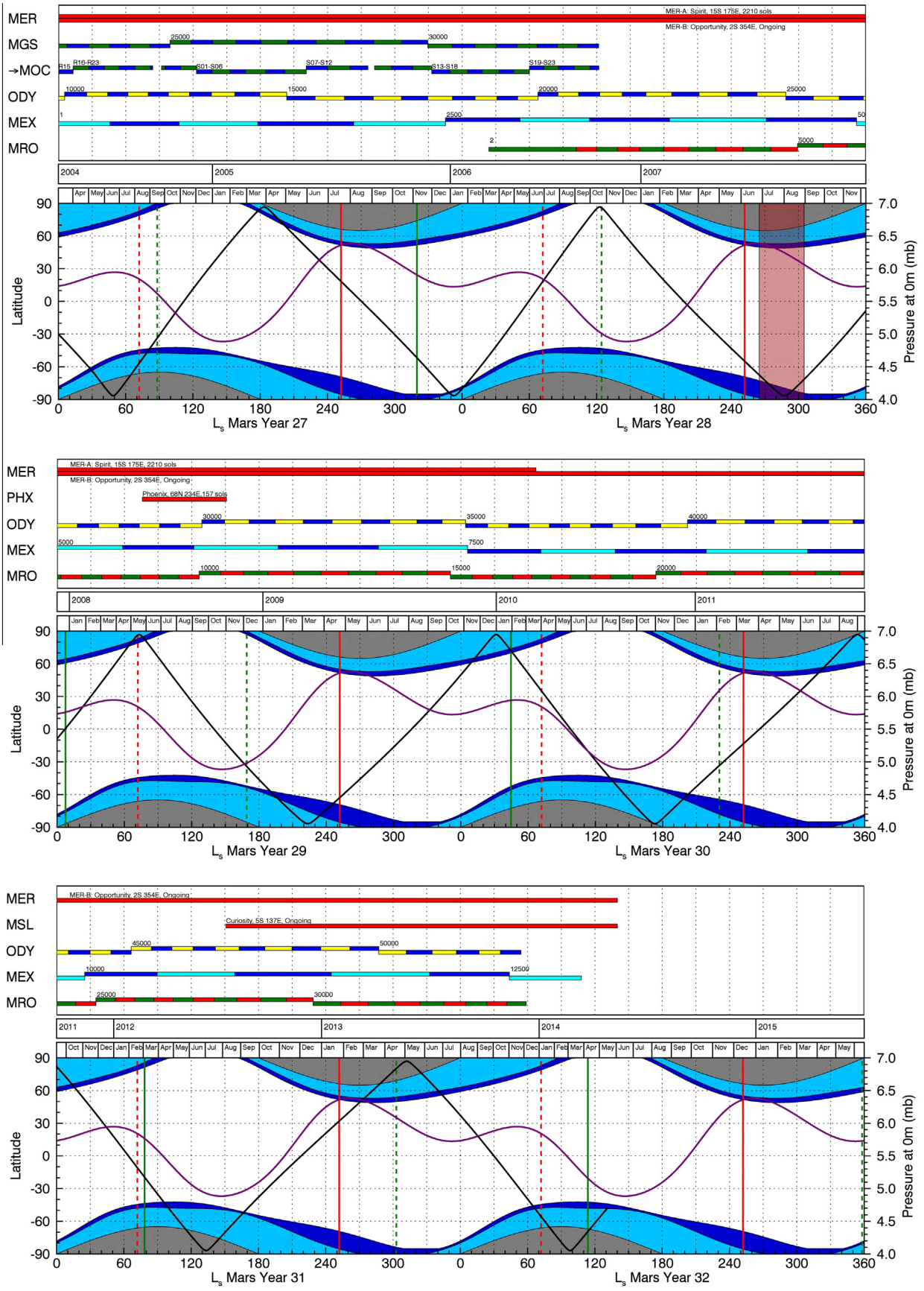

Fig. 1 (*continued*)

Table 1
Starting date of Mars years, as days from J2000, JD 2451545.

Mars year	Earth			Days from J2000	Mars year	Earth			Days from J2000	Mars year	Earth			Days from J2000
	Year	Mon	Day			Year	Mon	Day			Year	Mon	Day	
−184	1607	4	25	−143425.630	−89	1785	12	30	−78163.396	6	1964	9	5	−12901.180
−183	1609	3	12	−142738.650	−88	1787	11	17	−77476.419	7	1966	7	24	−12214.210
−182	1611	1	28	−142051.670	−87	1789	10	4	−76789.479	8	1968	6	10	−11527.270
−181	1612	12	15	−141364.720	−86	1791	8	21	−76102.520	9	1970	4	28	−10840.290
−180	1614	11	2	−140677.740	−85	1793	7	8	−75415.524	10	1972	3	15	−10153.300
−179	1616	9	19	−139990.750	−84	1795	5	26	−74728.550	11	1974	1	31	−9466.317
−178	1618	8	7	−139303.790	−83	1797	4	12	−74041.600	12	1975	12	19	−8779.349
−177	1620	6	24	−138616.820	−82	1799	2	28	−73354.610	13	1977	11	5	−8092.373
−176	1622	5	12	−137929.850	−81	1801	1	16	−72667.640	14	1979	9	23	−7405.432
−175	1624	3	29	−137242.910	−80	1802	12	4	−71980.690	15	1981	8	10	−6718.466
−174	1626	2	14	−136555.930	−79	1804	10	21	−71293.710	16	1983	6	28	−6031.469
−173	1628	1	2	−135868.920	−78	1806	9	8	−70606.720	17	1985	5	15	−5344.497
−172	1629	11	19	−135181.960	−77	1808	7	26	−69919.760	18	1987	4	1	−4657.544
−171	1631	10	7	−134495.002	−76	1810	6	13	−69232.790	19	1989	2	16	−3970.550
−170	1633	8	24	−133808.020	−75	1812	4	30	−68545.820	20	1991	1	4	−3283.590
−169	1635	7	12	−133121.080	−74	1814	3	18	−67858.880	21	1992	11	21	−2596.642
−168	1637	5	29	−132434.120	−73	1816	2	3	−67171.880	22	1994	10	9	−1909.654
−167	1639	4	16	−131747.120	−72	1817	12	21	−66484.880	23	1996	8	26	−1222.672
−166	1641	3	3	−131060.140	−71	1819	11	8	−65797.930	24	1998	7	14	−535.714
−165	1643	1	19	−130373.170	−70	1821	9	25	−65110.960	25	2000	5	31	151.264
−164	1644	12	6	−129686.190	−69	1823	8	13	−64423.980	26	2002	4	18	838.229
−163	1646	10	24	−128999.230	−68	1825	6	30	−63737.040	27	2004	3	5	1525.176
−162	1648	9	10	−128312.290	−67	1827	5	18	−63050.080	28	2006	1	21	2212.173
−161	1650	7	29	−127625.300	−66	1829	4	4	−62363.090	29	2007	12	9	2899.166
−160	1652	6	15	−126938.310	−65	1831	2	20	−61676.100	30	2009	10	26	3586.124
−159	1654	5	3	−126251.360	−64	1833	1	7	−60989.140	31	2011	9	13	4273.090
−158	1656	3	20	−125564.390	−63	1834	11	25	−60302.160	32	2013	7	31	4960.070
−157	1658	2	5	−124877.400	−62	1836	10	12	−59615.210	33	2015	6	18	5647.012
−156	1659	12	24	−124190.460	−61	1838	8	30	−58928.250	34	2017	5	5	6333.979
−155	1661	11	10	−123503.480	−60	1840	7	17	−58241.260	35	2019	3	23	7020.971
−154	1663	9	28	−122816.490	−59	1842	6	4	−57554.280	36	2021	2	7	7707.956
−153	1665	8	14	−122129.530	−58	1844	4	21	−56867.320	37	2022	12	26	8394.918
−152	1667	7	2	−121442.560	−57	1846	3	9	−56180.340	38	2024	11	12	9081.896
−151	1669	5	19	−120755.590	−56	1848	1	25	−55493.360	39	2026	9	30	9768.843
−150	1671	4	6	−120068.650	−55	1849	12	12	−54806.420	40	2028	8	17	10455.797
−149	1673	2	21	−119381.670	−54	1851	10	30	−54119.440	41	2030	7	5	11142.793
−148	1675	1	9	−118694.660	−53	1853	9	16	−53432.450	42	2032	5	22	11829.774
−147	1676	11	26	−118007.690	−52	1855	8	4	−52745.490	43	2034	4	9	12516.727
−146	1678	10	14	−117320.730	−51	1857	6	20	−52058.520	44	2036	2	25	13203.716
−145	1680	8	31	−116633.750	−50	1859	5	8	−51371.550	45	2038	1	12	13890.691
−144	1682	7	19	−115946.800	−49	1861	3	25	−50684.610	46	2039	11	30	14577.634
−143	1684	6	5	−115259.850	−48	1863	2	10	−49997.630	47	2041	10	17	15264.618
−142	1686	4	23	−114572.860	−47	1864	12	28	−49310.620	48	2043	9	4	15951.609
−141	1688	3	10	−113885.880	−46	1866	11	15	−48623.660	49	2045	7	22	16638.569
−140	1690	1	26	−113198.900	−45	1868	10	2	−47936.700	50	2047	6	9	17325.539
−139	1691	12	14	−112511.930	−44	1870	8	20	−47249.720	51	2049	4	26	18012.511
−138	1693	10	31	−111824.960	−43	1872	7	7	−46562.760	52	2051	3	13	18699.451
−137	1695	9	18	−111138.030	−42	1874	5	25	−45875.810	53	2053	1	28	19386.438
−136	1697	8	5	−110451.050	−41	1876	4	11	−45188.820	54	2054	12	16	20073.435
−135	1699	6	23	−109764.050	−40	1878	2	27	−44501.830	55	2056	11	2	20760.397
−134	1701	5	11	−109077.093	−39	1880	1	15	−43814.860	56	2058	9	20	21447.355
−133	1703	3	29	−108390.130	−38	1881	12	2	−43127.880	57	2060	8	7	22134.338
−132	1705	2	13	−107703.136	−37	1883	10	20	−42440.920	58	2062	6	25	22821.286
−131	1707	1	1	−107016.185	−36	1885	9	6	−41753.980	59	2064	5	12	23508.242
−130	1708	11	18	−106329.219	−35	1887	7	25	−41066.997	60	2066	3	30	24195.234
−129	1710	10	6	−105642.226	−34	1889	6	11	−40380.010	61	2068	2	15	24882.228
−128	1712	8	23	−104955.256	−33	1891	4	29	−39693.050	62	2070	1	2	25569.193
−127	1714	7	11	−104268.295	−32	1893	3	16	−39006.090	63	2071	11	20	26256.173
−126	1716	5	28	−103581.313	−31	1895	2	1	−38319.090	64	2073	10	7	26943.131
−125	1718	4	15	−102894.364	−30	1896	12	19	−37632.150	65	2075	8	25	27630.078
−124	1720	3	2	−102207.404	−29	1898	11	6	−36945.180	66	2077	7	12	28317.068
−123	1722	1	18	−101520.398	−28	1900	9	24	−36258.190	67	2079	5	30	29004.055
−122	1723	12	6	−100833.418	−27	1902	8	12	−35571.220	68	2081	4	16	29691.009
−121	1725	10	23	−100146.468	−26	1904	6	29	−34884.260	69	2083	3	4	30377.985
−120	1727	9	10	−99459.495	−25	1906	5	17	−34197.270	70	2085	1	19	31064.971
−119	1729	7	27	−98772.531	−24	1908	4	3	−33510.330	71	2086	12	7	31751.911
−118	1731	6	14	−98085.589	−23	1910	2	19	−32823.360	72	2088	10	24	32438.882

(*continued on next page*)

Table 1 (*continued*)

Mars year	Earth			Days from J2000	Mars year	Earth			Days from J2000	Mars year	Earth			Days from J2000
	Year	Mon	Day			Year	Mon	Day			Year	Mon	Day	
−117	1733	5	1	−97398.606	−22	1912	1	7	−32136.350	73	2090	9	11	33125.875
−116	1735	3	19	−96711.617	−21	1913	11	24	−31449.370	74	2092	7	29	33812.839
−115	1737	2	3	−96024.640	−20	1915	10	12	−30762.420	75	2094	6	16	34499.801
−114	1738	12	22	−95337.666	−19	1917	8	29	−30075.450	76	2096	5	3	35186.780
−113	1740	11	8	−94650.693	−18	1919	7	17	−29388.490	77	2098	3	21	35873.724
−112	1742	9	26	−93963.755	−17	1921	6	2	−28701.540	78	2100	2	6	36560.703
−111	1744	8	13	−93276.782	−16	1923	4	20	−28014.560	79	2101	12	25	37247.706
−110	1746	7	1	−92589.784	−15	1925	3	7	−27327.570	80	2103	11	12	37934.680
−109	1748	5	18	−91902.815	−14	1927	1	23	−26640.590	81	2105	9	29	38621.635
−108	1750	4	5	−91215.857	−13	1928	12	10	−25953.620	82	2107	8	17	39308.617
−107	1752	2	21	−90528.864	−12	1930	10	28	−25266.650	83	2109	7	4	39995.576
−106	1754	1	8	−89841.907	−11	1932	9	14	−24579.710	84	2111	5	22	40682.523
−105	1755	11	26	−89154.953	−10	1934	8	2	−23892.740	85	2113	4	8	41369.510
−104	1757	10	13	−88467.964	−9	1936	6	19	−23205.740	86	2115	2	24	42056.507
−103	1759	8	31	−87780.989	−8	1938	5	7	−22518.780	87	2117	1	10	42743.474
−102	1761	7	18	−87094.033	−7	1940	3	24	−21831.820	88	2118	11	28	43430.445
−101	1763	6	5	−86407.054	−6	1942	2	9	−21144.820	89	2120	10	15	44117.411
−100	1765	4	22	−85720.096	−5	1943	12	28	−20457.870	90	2122	9	2	44804.349
−99	1767	3	10	−85033.149	−4	1945	11	14	−19770.910	91	2124	7	20	45491.328
−98	1769	1	25	−84346.147	−3	1947	10	2	−19083.920	92	2126	6	7	46178.320
−97	1770	12	13	−83659.157	−2	1949	8	19	−18396.940	93	2128	4	24	46865.281
−96	1772	10	30	−82972.202	−1	1951	7	7	−17709.980	94	2130	3	12	47552.248
−95	1774	9	17	−82285.232	0	1953	5	24	−17023.002	95	2132	1	28	48239.246
−94	1776	8	4	−81598.256	1	1955	4	11	−16336.050	96	2133	12	15	48926.192
−93	1778	6	22	−80911.313	2	1957	2	26	−15649.090	97	2135	11	2	49613.155
−92	1780	5	9	−80224.337	3	1959	1	14	−14962.090	98	2137	9	19	50300.150
−91	1782	3	27	−79537.345	4	1960	12	1	−14275.110	99	2139	8	7	50987.124
−90	1784	2	12	−78850.365	5	1962	10	19	−13588.160	100	2141	6	24	51674.083

Fig. 1 therein shows the progression of seasons through a Martian year. Allison and McEwen (2000) present the date (as JD-2400000.5) of $L_s = 0°$ over 1874–2126 but start the count of Mars years in 1874. Both of those prior results and Table 1 used the Mars pole orientation known at the time; each slightly different. To obtain accuracy and smoothness over long periods, precise definition of the orbit plane and the spin-axis direction are needed because perturbations by the other planets results in small irregularities in Mars heliocentric position both along and normal to the "average" orbit plane. The heliocentric position of Mars is based on planetary and lunar ephemerides DE430 (Folkner et al., 2014) which uses the International Celestial Reference System, IRCS, and includes the effect of all planets, all significant satellites and the largest several hundred asteroids. All calculations are in ephemeris time (Barycentric Dynamical Time, TDB) and results in Table 1 are shown in ephemeris days relative to 2451545, which is epoch J2000.0 (2000 January 1, 12 hour). To generate Table 1, the normal to the orbit plane is computed based on a least-squares fit quadratic in time to the instantaneous cross-product of the heliocentric position and velocity of Mars evaluated for many seasons each year:

$$\begin{aligned} \mathrm{RA} &= 273^\circ.373218337 - 0.02985932966T - 4.829810557\times10^{-5}T^2 \\ \mathrm{Dec} &= 65^\circ.322934512 - 0.00128897471T + 4.460153556\times10^{-5}T^2 \end{aligned} \quad (1)$$

with *RA* the right ascension (°), *Dec* the declination (°), and *T* the Julian centuries from epoch J2000.0. Calculation of the vernal equinox also requires the direction along the spin axis of the planet; here the determination of Kuchynka et al. (2014) is used, also in the ICRF, but omitting terms with a period of one Mars year or less, all <0.00024°. Including those short-period terms advances the date of $L_s = 0$ by $0.000377 \pm 3.22 \times 10^{-6}$ days, but would yield a vernal-equinox direction that oscillates through a MY.

The nomenclature and time referencing of the various datasets acquired throughout the robotic exploration of Mars are generally instrument-specific and often related to spacecraft internal clocks, orbit numbers or Julian Dates, with little reference to Mars time (seasons or years). Consequently, fast and straightforward identification of mission/instrument duration and overlap in the context of long-term observational studies is not easy. To address this gap, Fig. 1 provides an overview of major robotic exploration events since the arrival of Mars Pathfinder, along with global scale processes (e.g., latitudinal extent of the polar night, surface atmospheric pressure at 0 m elevation, climatological seasonal polar cap edges, etc.) in a format centered on Mars time (L_s and MY) as proposed in Table 1. Fig. 1starts after a hiatus of two decades in spacecraft exploration following the Viking missions. Similar information for all Mars spacecraft not included in Fig. 1 are given by Snyder and Moroz (1992).

All analytic expressions for L_S here are empirical derived by fitting 285 Mars Years from 1607 to 2143. They are based on fits to minimize the root-mean-square (RMS) residual at 36 times per Mars year uniformly spaced over the entire interval and use a form similar to Allison [2000].

The linear-rate angle based on the tropical year is α where t is the ephemeris time from J2000.0 in days.

$$\alpha = a_0 + a_1 t + a_2 T^2 \sim 270.389001822 + 0.52403850205\ t - 0.000565452\ T^2 \quad (2)$$

$$M = m_0 + m_1 t \sim 19.38028331517 + 0.52402076345\ t \quad (3)$$

where M is the mean anomaly. Using eccentricity e defined as

$$e = e_0 + e_1 T \sim 0.093402202 + 0.000091406\ T \quad (4)$$

Table 2
Planetary perturbation terms. 2*E*-3*M* is shorthand for $1/(E/2 - M/3)$ where *E* is the length of a year for Earth, *M* for Mars, *J* for Jupiter and *V* for Venus. Years are based on the semi-major axes at epoch J2000 given by Standish and Williams (2006).

Planets	Commensurate years	Period days τ_i	Amplitude milli-deg $1000A_i$	Phase degree φ_i
M-J	2.23511	816.3755210	7.0591	48.48944
M-2J	2.75373	1005.8002614	6.0890	167.55418
2M-2J	1.11756	408.1877605	4.4462	188.35480
2M-E	15.78456	5765.3098103	3.8947	19.97295
E-M	2.13533	779.9286472	2.4328	12.03224
2E-3M	2.46939	901.9431281	2.0400	95.98253
V-3M	32.80201	11980.9332471	1.7746	49.00256
4M-2E	7.89228	2882.1147	1.34607	288.7737
*(2M-E) * 3/4*	9.06113	4332.2204	1.03438	37.9378
2M-J	1.02138	373.07883	0.88180	65.3160
5M-3E	2.92735	1069.3231	0.72350	175.4911
M-V	0.91423	343.49194	0.65555	98.8644
M-3J	3.58573	1309.9410	0.81460	186.2253
2M-3J	1.23373	450.69255	0.74578	202.9323
3M-2J	0.70103	256.06036	0.58359	212.1853
3M-S	0.64060	228.99145	0.42864	32.1227

to evaluate the true anomaly v using the equation of center yields:

$$\Delta \equiv v - M = \left(2e - \frac{e^3}{4} + \frac{5e^5}{96}\right) sin(M) + \left(\frac{5e^2}{4} - \frac{11e^4}{24} + \frac{17e^6}{192}\right) sin(2M) + \left(\frac{13e^3}{12} - \frac{43e^5}{64}\right) sin(3M) + \left(\frac{103e^4}{96} - \frac{451e^6}{480}\right) sin(4M) + \frac{1097e^5}{960} sin(5M) + \frac{1223e^5}{960} sin(6M) + O(e^7) \quad (5)$$

Major perturbations by other planets are treated as:

$$PP_S = \sum_{i=1}^{N} A_i cos\left[2\pi \frac{t}{\tau_i} + \frac{\pi}{180}\phi_i\right] \quad (6)$$

where τ is the commensurate period in days and ϕ is phase in degrees; coefficient values are given in Table 2.

$$L_s = \alpha + \frac{180}{\pi}\Delta + PP_s \quad (7)$$

Using only the first seven terms in Table 2, this model is adequate to match the DE430 calculations with maximum error of 0.0073° over the 536 years of MY −184 through MY 100; the RMS residual is 0.00207°. With all terms in Table 2, the maximum error is 0.0045° and the RMS residual is 0.00105°.

A simpler relation is within 0.05° over the entire period:

$$\mathrm{M} = 19.38095 + 0.524020769\ t \quad (8)$$

$$\mathrm{L_S} \sim 270.38859 + 0.524038542\ t + 10.67848\ \mathrm{sin(M)} + 0.62077\ \mathrm{sin(2M)} + 0.05031\ \mathrm{sin(3M)} \quad (9)$$

With this document, we extend the enumeration of MY proposed by Clancy et al. (2000) and provide the community with a practical reference for time keeping on Mars needed for studies of long-term and inter-annual phenomena. A numerical tool located at http://krc.mars.asu.edu/LsTool/ has been developed to compute L_s as a function of the date.

Acknowledgments

Work at the Jet Propulsion Laboratory, California Institute of Technology was performed under a contract with the National Aeronautics and Space Administration. SP would like to thank Armin Kleinböhl for his valuable suggestions and constructive comments. HK thanks Myles Standish and the NAIF group at JPL for development of, and ready access to, the software and data files of the planetary and lunar ephemerides. We also thank two reviewers, and our colleagues who have participated in the discussions that lead to the genesis of this paper:

Adrian Brown, Frank Seelos, Jack Holt, Janice Bishop, Jim Bell, Jack Mustard, Ken Herkenhoff, Kim Seelos, Alfred McEwen, Nicholas Thomas, Patrick Russell, Phil James, Jeff Plaut, Ralph Milliken, Peter Thomas, Sara Christian, Wendy Calvin, Nathaniel Putzig, Anton Ivanov, Sarah Milkovich, Roger Philips, Daniel Nunes, Philip Christensen, Andy McGovern, Yves Langevin, Liliya Posiolova, Giovanni Alberti, Roberto Seu, Claudio Catallo, Jonathon Hill, Isaac Smith, Thomas Brothers, Jonathan Bapst, Margaret Landis, Patricio Becerra, Ali Bramson, Ganna Portyankina, and Paul Hayne.

References

Allison, M., McEwen, M., 2000. A post-Pathfinder evaluation of areocentric solar coordinates with improved timing recipes for Mars seasonal/diurnal climate studies. Planet. Space Sci. 48 (2–3), 215–235.

Antoniadi, E.M., 1930. La Planete Mars. Hermann, Paris.

Benson, J.L., James, P.B., Cantor, B.A., Remigio, R., 2006. Interannual variability of water ice clouds over major martian volcanoes observed by MOC. Icarus 184 (2), 365–371.

Byrne, S., Ingersoll, A.P., 2003. A sublimation model for martian south polar ice features. Science 299, 1051–1053.

Byrne, S. et al., 2009. Distribution of mid-latitude ground ice on Mars from new impact craters. Science 325 (5948), 1674–1676. http://dx.doi.org/10.1126/science.1175307.

Clancy, R.T. et al., 2000. An intercomparison of ground-based millimeter, MGS TES, and Viking atmospheric temperature measurements: Seasonal and interannual variability of temperatures and dust loading in the global Mars atmosphere. J. Geophys. Res. 105, 9553–9572.

Daubar, I.J., McEwen, A.S., Byrne, S., Kennedy, M.R., Ivanov, B., 2013. The current martian cratering rate. Icarus 225 (1), 506–516. http://dx.doi.org/10.1016/j.icarus.2013.04.009.

de Vaucouleurs, G., 1954. Physics of the Planet Mars. Faber and Faber Ltd..

Florenski, C.P., Basilevski, A.T., Kuzmin, R.O., Chernaya, I.M., 1975. Geomorphologic analysis of some martian surface images from the Mars 4 and 5 automatic stations. Icarus 26 (2), 219–229.

Folkner, W.M., Williams, J.G., Boggs, D.H., Park, R.S., Kuchynka, P., 2014. The Planetary and Lunar Ephemerides DE430 and DE431. The Interplanetary Network Progress Report, 42(196).

Geissler, P.E., 2005. Three decades of martian surface changes. J. Geophys. Res. 110, E02001. http://dx.doi.org/10.1029/2004JE002345.

Golitsyn, G.S., 1973. On the martian dust storms. Icarus 18, 113–119.

Hansen, C.J. et al., 2011. Seasonal erosion and restoration of Mars' northern polar dunes. Science 331 (6017), 575–578. http://dx.doi.org/10.1126/science.1197636.

James, P.B., Kieffer, H.H., Paige, D.A., 1992. The seasonal cycle of carbon dioxide on Mars. In: Kieffer, H.H., Jakosky, B.M., Snyder, C.W., Matthews, M.M. (Eds.), Mars. Univ. of Arizona Press, Tucson.

Kieffer, H.H., Jaskosky, B.M., Snyder, C.W., 1992. The planet Mars, from antiquity to the present. In: Kieffer, H.H. et al. (Eds.), Mars. Univ. of Arizona Press, Tucson, pp. 1–33.

Kuchynka, P., Folkner, W.M., Konopliv, A.S., Parker, T.J., Le Maistre, S., Dehant, V., 2014. New constraints on Mars rotation determined from radiometric tracking of the Opportunity Mars Exploration Rover. Icarus 229, 340–347. http://dx.doi.org/10.1016/j.icarus.2013.11.015.

Leighton, R.B., Murray, B.C., Sharp, R.P., Allen, J.D., Sloan, R.K., 1965. Mariner IV photography of Mars: Initial results. Science 149, 627–630.
Mangold, N. et al., 2010. Sinuous gullies on Mars: Frequency, distribution, and implications for flow properties. J. Geophys. Res. 115, E11001. http://dx.doi.org/10.1029/2009je003540.
Martin, L.J., Baum, W.A., 1969. A Study of Cloud Motions on Mars. Lowell Observatory Report, August.
Martin, L.J., James, P.B., Dollfus, A., Iwasaki, K., Beish, J.D., 1992. Telescopic observations: Visual, photographic, polarimetric. In: Kieffer, H.H. et al. (Eds.), Mars. Univ. of Arizona Press, Tucson, pp. 34–70.
McEwen, A.S. et al., 2011. Seasonal flows on warm martian slopes. Science 333 (6043), 740–743. http://dx.doi.org/10.1126/science.1204816.
Michaels, T.I., 2006. Numerical modeling of Mars dust devils: Albedo track generation. Geophys. Res. Lett. 33, L19S08. http://dx.doi.org/10.1029/2006GL026268.
Rafkin, S.C.R., Haberle, R.M., Michaels, T.I., 2001. The Mars regional atmospheric modeling system: Model description and selected simulations. Icarus 151 (2), 228–256.
Russell, P. et al., 2008. Seasonally active frost-dust avalanches on a north polar scarp of Mars captured by HiRISE. Geophys. Res. Lett. 35 (23), L23204. http://dx.doi.org/10.1029/2008gl035790.
Slipher, E.C., 1927. Atmospheric and surface phenomena on Mars. Publ. Astron. Soc. Pacific 39, 209–216.
Slipher, E.C., 1962. The Photographic Atlas of Mars. Sky Publishing Corporation, Cambridge, Mass, 168pp.
Smith, M.D., 2004. Interannual variability in TES atmospheric observations of Mars during 1999–2003. Icarus 167, 148–165.
Smith, D.E., Zuber, M.T., Neumann, G.A., 2001. Seasonal variations of snow depth on Mars. Science 294, 2141–2146.
Snyder, C.W., Moroz, V.I., 1992. Spacecraft exploration of Mars. In: Kieffer, H.H. et al. (Eds.), Mars. Univ. of Arizona Press, Tucson, pp. 71–119.
Soderblom, L.A., Bell, J., 2008. Exploration of the martian surface: 1992–2007. In: Bell, J.F., III (Ed.), The Martian Surface: Composition, Mineralogy, and Physical Properties. Cambridge University Press, New York, pp. 3–19.
Standish, E.M., Williams, J.G., 2006. Keplerian elements of the approximate positions of the major planets. In: Seidelmann, K.P. (Ed.), Explanatory Supplement to the Astronomical Almanac, Washington D.C.
Sullivan, R., Thomas, P., Veverka, J., Malin, M., Edgett, K.S., 2001. Mass movement slope streaks imaged by the Mars Orbiter Camera. J. Geophys. Res. 106 (E10), 23607–23633.
Tamppari, L.K., Zurek, R.W., Paige, D.A., 2000. Viking era water ice clouds. J. Geophys. Res. 105, 4087–4107.
Thomas, P.C., James, P.B., Calvin, W.M., Haberle, R., Malin, M.C., 2009. Residual south polar cap of Mars: Stratigraphy, history, and implications of recent changes. Icarus 203 (2), 352–375. http://dx.doi.org/10.1016/j.icarus.2009.05.014.
Tillman, J.E., Johnson, N.C., Guttorp, P., Percival, D.B., 1993. The martian annual atmospheric pressure cycle: Years without great dust storms. J. Geophys. Res. 98, 10963–10971.
Titus, T.N., 2005. Mars polar cap edges tracked over 3 full Mars years. Proc. Lunar Sci. Conf. 36.
Titus, T.N., Calvin, W.N., Kieffer, H.H., Langevin, Y., Prettyman, T.H., 2008. Martian polar processes. In: Bell, J.F., III (Ed.), The Martian Surface: Composition, Mineralogy and Physical Properties. Cambridge University Press, pp. 578–598.
Verba, C.A., Geissler, P.E., Titus, T.N., Waller, D., 2010. Observations from the High Resolution Imaging Science Experiment (HiRISE): Martian dust devils in Gusev and Russell craters. J. Geophys. Res. 115, E09002. http://dx.doi.org/10.1029/2009je003498.
Wood, S.E., Paige, D.A., 1992. Modeling the martian seasonal CO_2 cycle 1. Fitting the Viking Lander pressure curves. Icarus 99 (1), 1–14.
Wright, W.H., Kuiper, G.P., 1935. Clouds on Mars. Publ. Astron. Soc. Pacific 47, 92–93.